Supplementary Information

Boosting Electrochemical Reaction and Suppressing Phase Transition with High-Entropy O3-Type Layered Oxide for Sodium-Ion Batteries

Kanghui Tian, [a] Huan He, [a] Xiao Li, [a] Dan Wang, [a,b] Zhiyuan Wang,*[a,b] Runguo Zheng, [a,b]

Hongyu Sun, [b] Yanguo Liu, [a,b] Qin-Chao Wang *[c]

[a] School of Materials Science and Engineering, Northeastern University, Shenyang 110819, P.R. China;

[b] School of Resources and Materials, Northeastern University at Qinhuangdao, Qinhuangdao 066004, P.R.China;

[c]School of Chemistry and Chemical Engineering, Yangzhou University, Jiangsu 225002, P. R. China;

Corresponding author: (ZYW) zhiyuanwang@neuq.edu.cn; (Q-C W) wangqinchao@yzu.edu.cn

Selection criteria for elements in O3-NFCNTSL HEO cathodes:

The selection criteria of elements in the design of the O3-NFCNTSL HEO cathode mainly include the following two points: Firstly, in order to design the HEO cathode, it is necessary to form the translation metal disordering, which is mainly controlled by the different in the ionic radii of transition metal. In common, large difference in ionic radii is favorable for forming ordered arrangement, while small difference tends to form disordered arrangement. Here, the ionic radii of selected element (Fe^{3+}, Ni^{2+}, Co^{3+}, Mn^{4+}, Ti^{4+}, Sn^{4+}) is smaller than 15%, so it is easily to synthesize the disordering of transition metal. For Li^{+}, it is easily to occupy the Ni^{2+} sites, such as Li^{+}/Ni^{2+} cation mixing in $LiNi_{1-x-y}Mn_xCoO_2$ system. So those selected cationic elements can from the disordering of transition metal; Secondly, the selected elements must be providing the charge compensation, which can enhance electrochemical performance. Although Ti^{4+} and Sn^{4+} are electrochemically inactive, they also play an important role to stabilize the structure of O3. For Ti^{4+}, the diffused Ti 3*d* orbitals can from strong Ti-TM interactions between two adjacent edge sharing TM-O_6 and Ti-O_6 octahedrals. It is pervious reported that introducing Ti in O3 structure might be able to suppress the migration of Fe by changing the local electronic structures, which is quite beneficial for the long-term cycling performance of the Fe-contained layered cathode [1,2]. We choice for Sn^{4+} lies in its inability to interact with oxygen through its *d* orbitals, hence reducing orbital overlap and favoring charge localization in the transition metal layer. This effect, combined with the concomitant increase of bond ionicity, should be beneficial to increase the redox potential [3,4]. In our manuscript, the substitution of Li can promote the reversible capacity of Na storage, as well as the long-term cycling and rate performance [5]. The radii and electrochemical effects of metal ions are shown in Table S1.

Na-ion diffusion coefficients calculation based on CV curves with different scan rates:

The Na-ion diffusion coefficients of O3-NFCNTSL electrode can be calculated according to the *Randles-Sevcik* equation:

$$I_p = 0.4463n^{3/2}F^{3/2}CSR^{-1/2}T^{-1/2}{D_{cv}}^{1/2}v^{1/2} \quad (1)$$

Where I_p (A) is the peak current, n is the number of electrons, F is the Faraday constant (96485 C mol^{-1}), C (mol cm^{-3}) is the bulk concentration, S (cm^2) is the area of the electrode, R is the gas constant (8.314 J mol^{-1} K^{-1}), T (K) is the absolute temperature, D_{cv} (cm^2 s^{-1}) is the Na-ion diffusion coefficient and v (V s^{-1}) is the scan rate. The ratio of I_p to $v^{1/2}$ is shown as the slope in Table S7.

Na-ion diffusion coefficients calculation based on GITT:

The electrochemical kinetics of the O3-NFCNTSL electrode was further investigated by GITT to determine the Na-ion diffusion coefficients. GITT was measured at LAND CT2001A instrument with a repeated pulses current of 0.05 C for 30 min, and the relaxation time is 4 h between each pulse.

The Na-ion diffusion coefficients of O3-NFCNTSL electrode can be calculated according to the following equation:

$$D = \frac{4}{\pi}\left(\frac{iV_m}{z_A FS}\right)^2\left(\frac{\Delta E_s/t}{dE_t/d\sqrt{t}}\right)^2 \quad (2)$$

When the E_τ and $\tau^{1/2}$ follow a linear relationship as shown in Figure 4c, the above formula can be simplified to:

$$D = \frac{4}{\pi\tau}\left(\frac{m_B V_M}{M_B S}\right)^2\left(\frac{\Delta E_s}{\Delta E_\tau}\right)^2 \ (\tau << L^2/D) \quad (3)$$

Where D (cm^2 s^{-1}) is the Na-ion diffusion coefficients, i (A) is the applied current, V_M (cm^3 mol^{-1}) is the molar volume, Z_A is the charge number of Na-ion, F is the Faraday constant (96485 C mol^{-1}), S (cm^2) is the surface area of the electrode, ΔEs is the voltage change caused by the pulse, ΔE_τ is the total change of the cell voltage E during the current pulse process, τ is the duration time of the current pulse and L (cm) is the diffusion length.

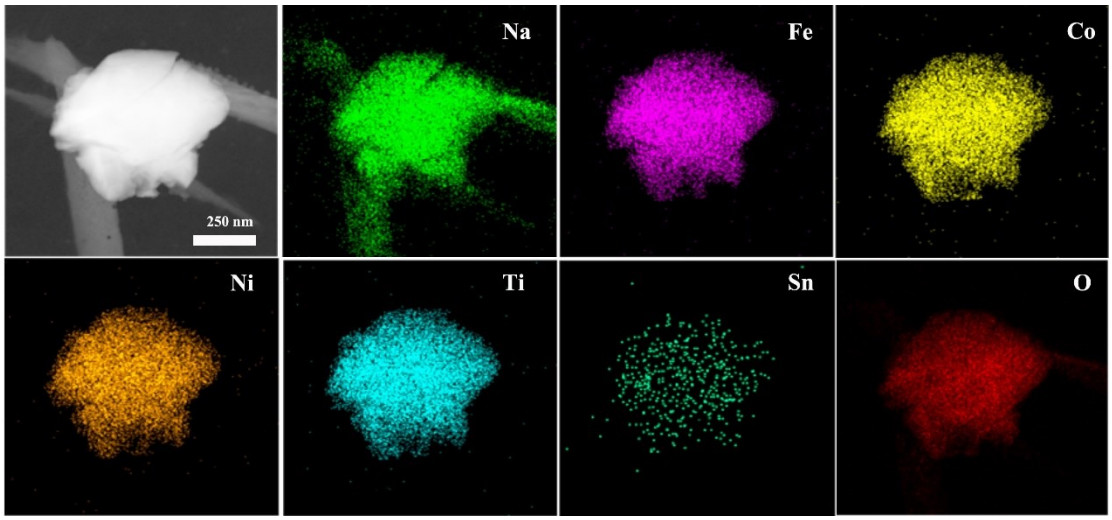

Fig. S1 TEM-EDS mappings for the O3-NFCNTSL cathode.

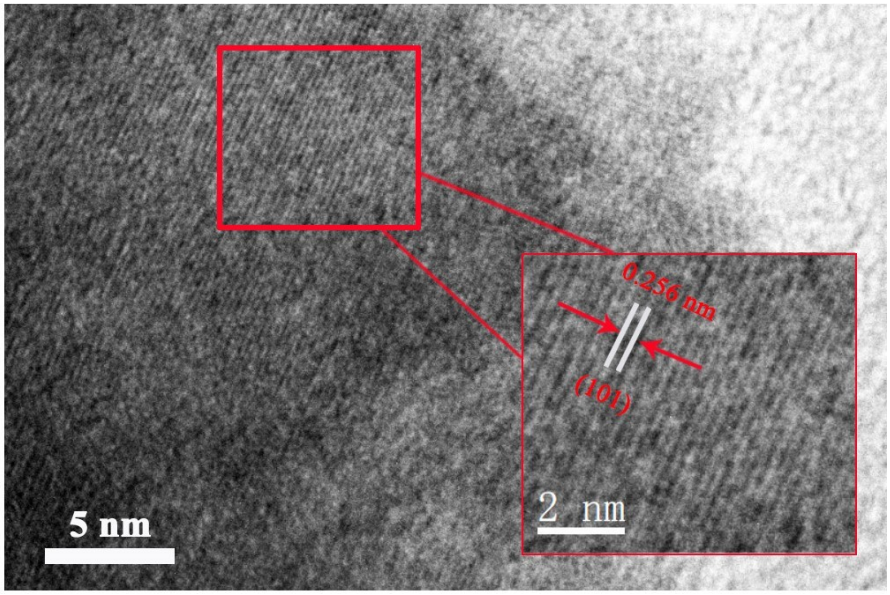

Fig. S2 HRTEM image of O3-NFCNTSL.

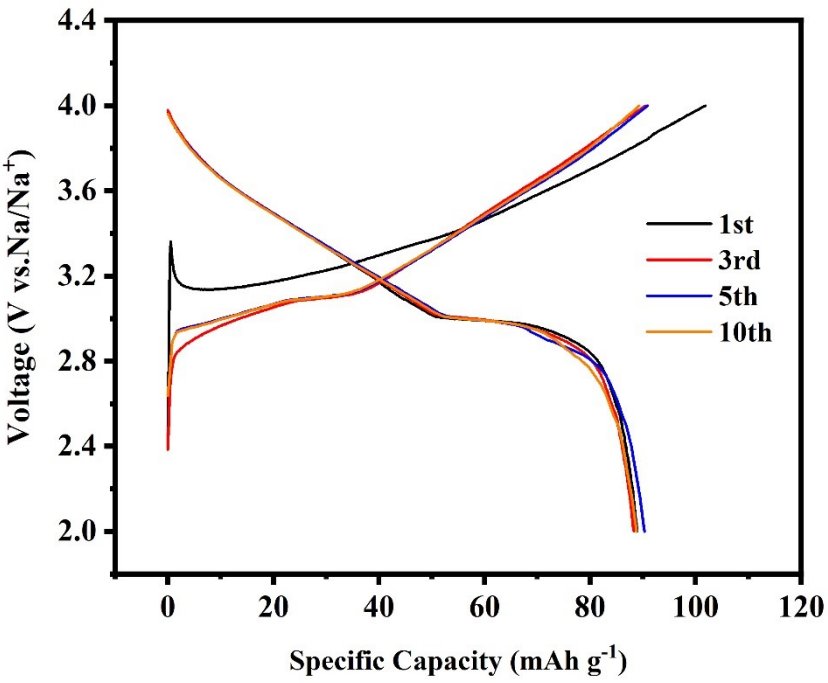

Fig. S3 Corresponding charge-discharge curves of the O3-NFCNTSL electrode in the voltage range of 2.0-4.0 V during 10 cycles at 0.1C.

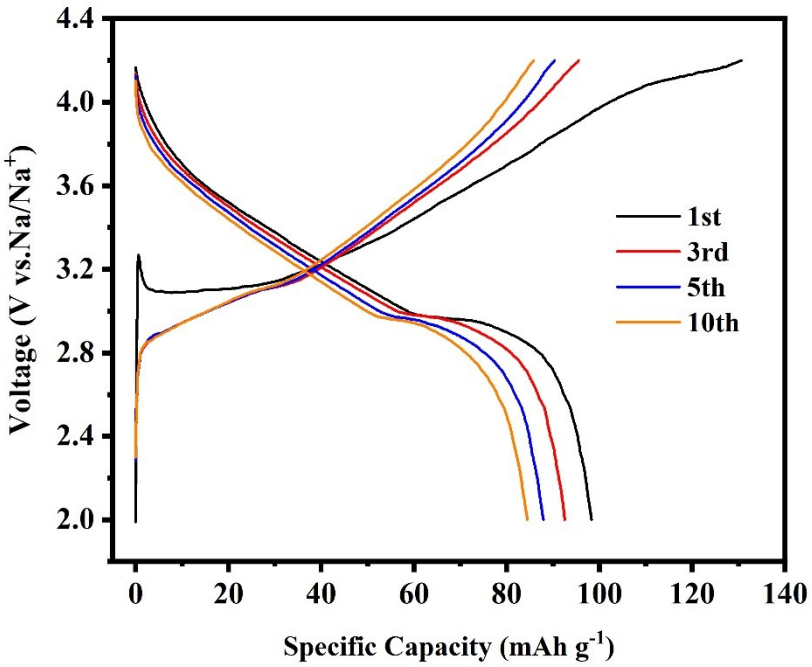

Fig. S4 Corresponding charge-discharge curves of the O3-NFCNTSL electrode in the voltage range of 2.0-4.2 V during 10 cycles at 0.1C.

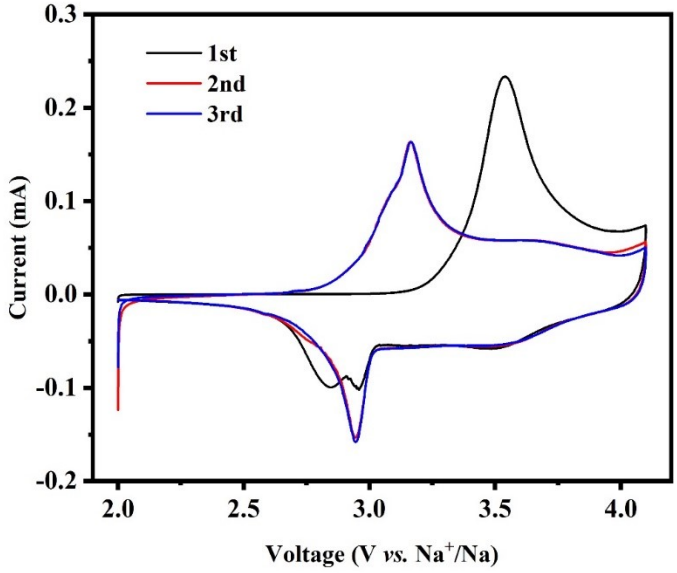

Fig. S5 The CV curves of O3-NFCNTSL for 1st, 2nd, and 3rd cycles obtained at a scan rate of 0.1 mV s^{-1}.

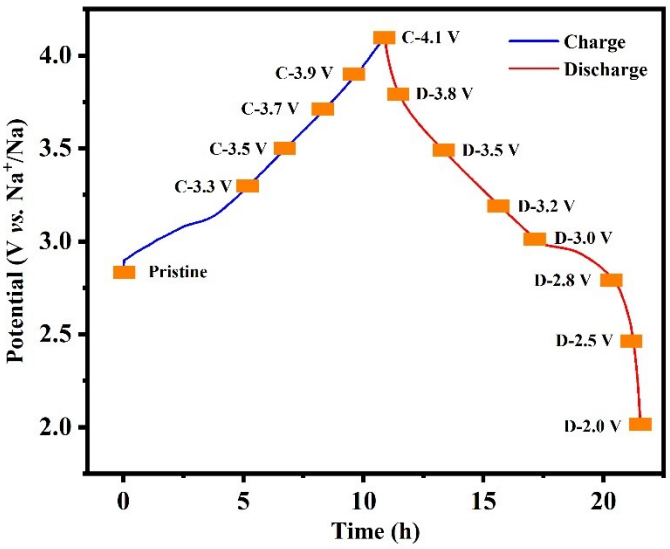

Fig. S6 Charge and discharge curves of O3-NFCNTSL electrode, orange solid squares on the curves stand for the state where ex-situ XRD data is obtained.

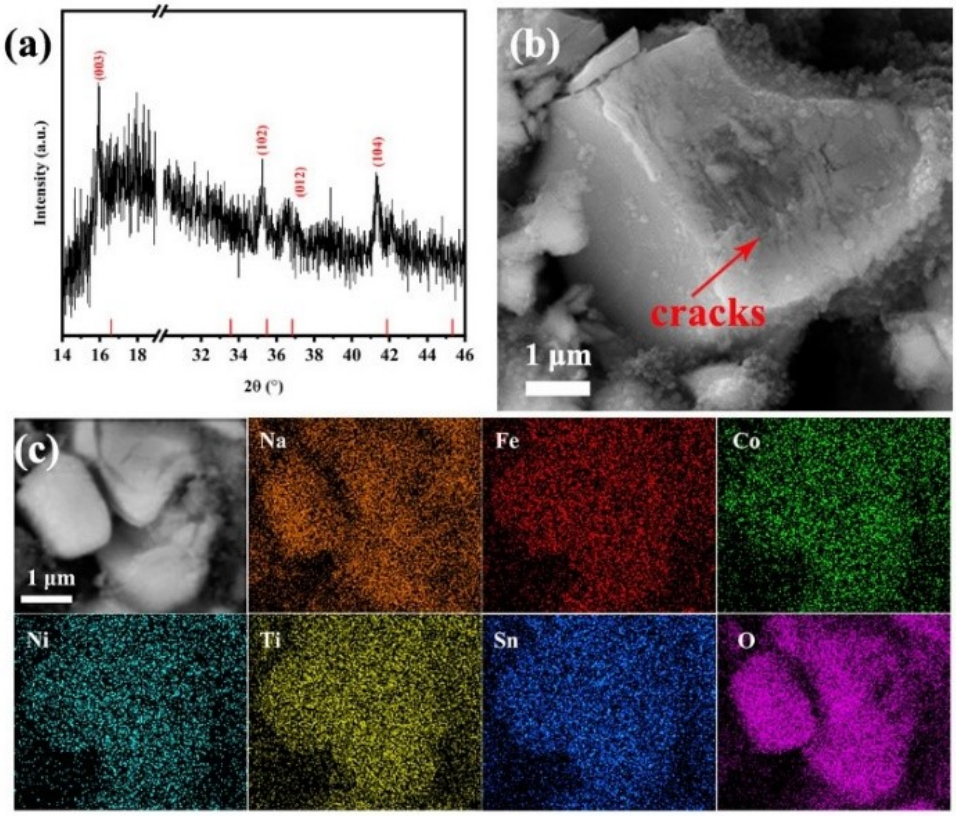

Fig. S7 The structure and morphology of the O3-NFCNTSL electrode after 100 cycles in the voltage range of 2.0-4.1V. (a) XRD pattern. (b) SEM image. (c) SEM-EDS mapping of all elements.

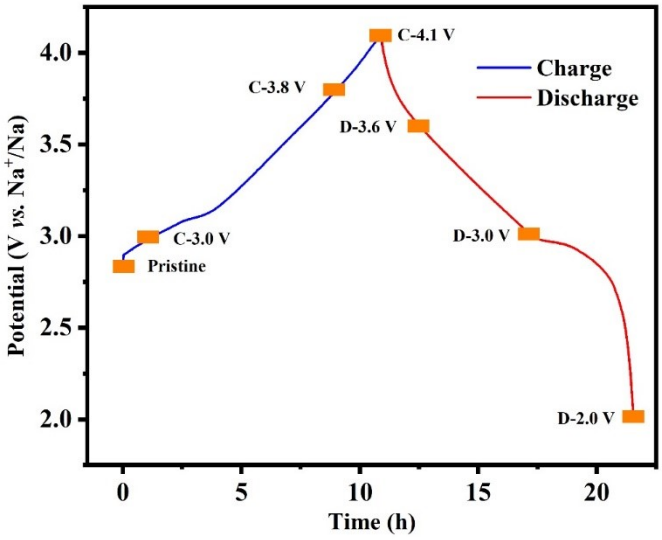

Fig. S8 Charge and discharge curves of O3-NFCNTSL electrode, orange solid squares on the curves stand for the state where XAS data is obtained.

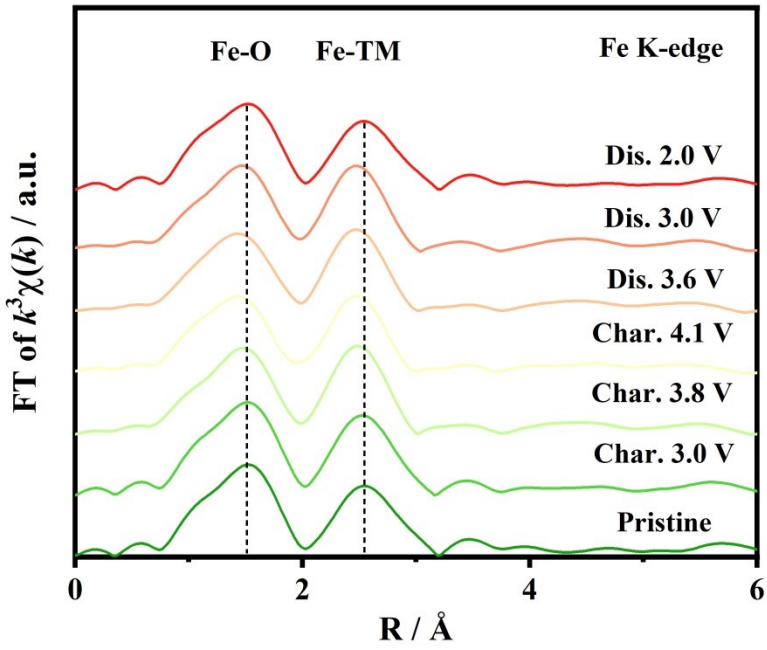

Fig. S9 Fe K-edge Fourier transformed EXAFS spectra of the O3-NFCNTSL at various states during the first charge (green) and first discharge (red) processes.

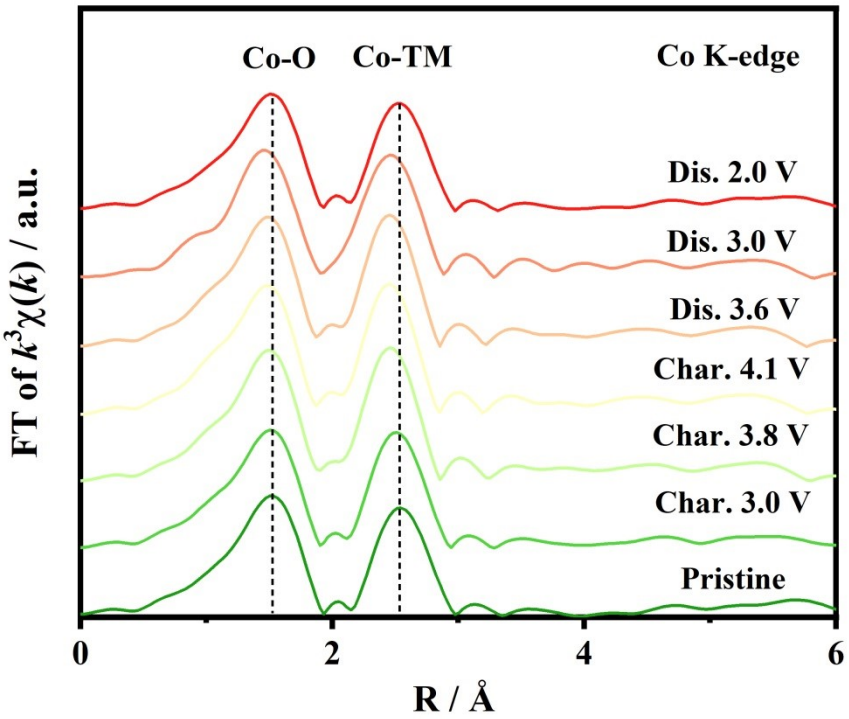

Fig. S10 Co K-edge Fourier transformed EXAFS spectra of the O3-NFCNTSL at various states during the first charge (green) and first discharge (red) processes.

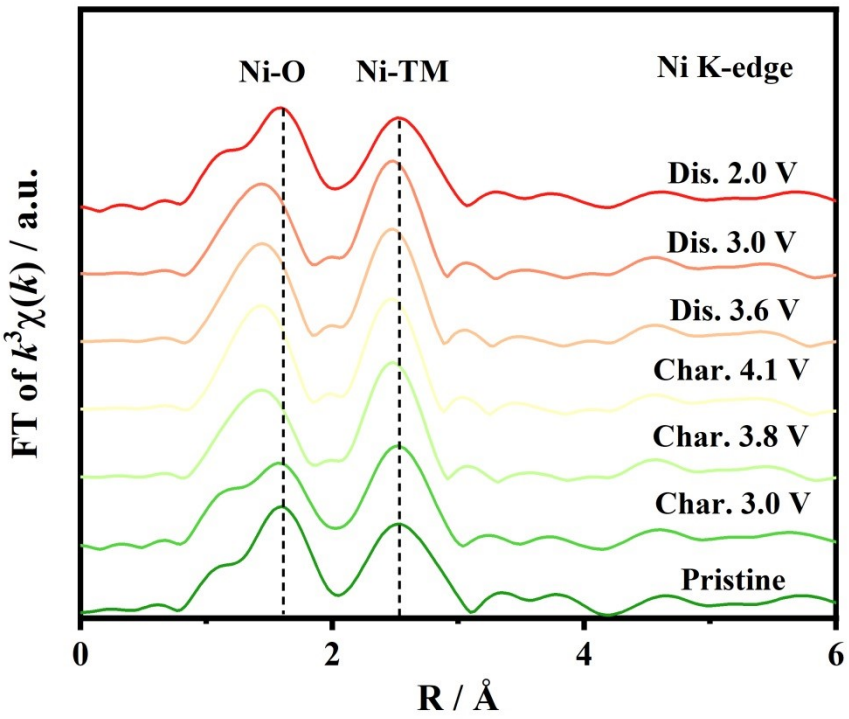

Fig. S11 Ni K-edge Fourier transformed EXAFS spectra of the O3-NFCNTSL at various states during the first charge and first discharge processes.

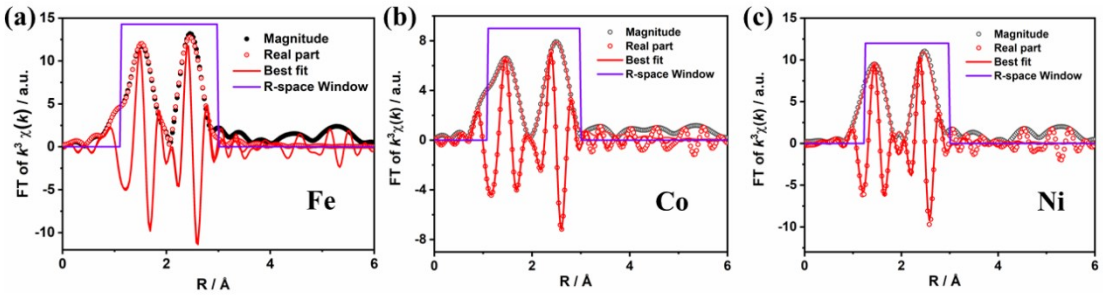

Fig. S12 Least-square fits of the calculated FT-EXAFS phase and amplitude functions to the experimental EXAFS spectra for Fe (a), Co(b), and Ni (c) at full charge of 4.1 V using P3 structure for fitting.

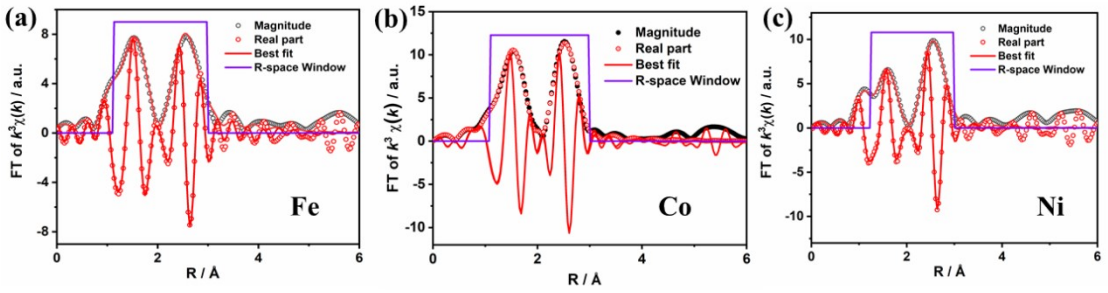

Fig. S13 Least-square fits of the calculated FT-EXAFS phase and amplitude functions to the experimental EXAFS spectra for Fe (a), Co(b), and Ni (c) at full discharge of 2.0 V using O3 structure for fitting.

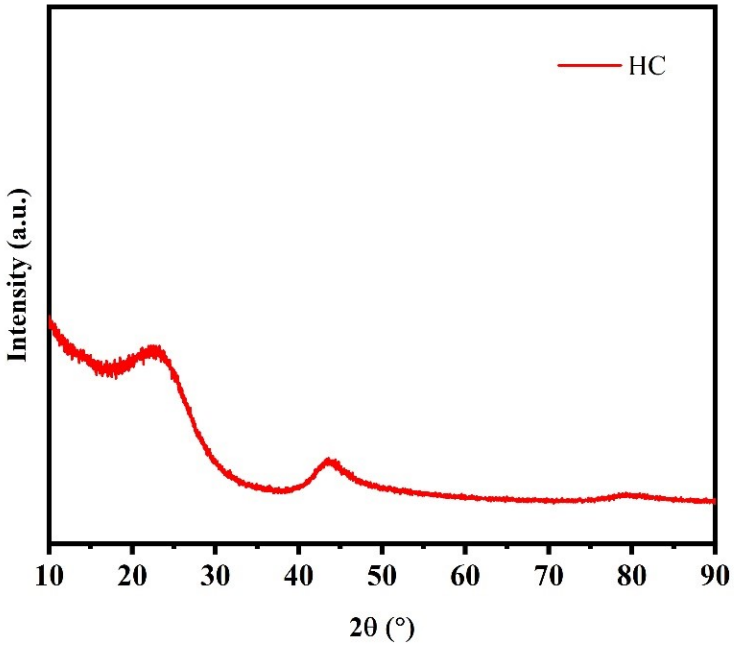

Fig. S14 XRD pattern of hard carbon anode.

Fig. S15 SEM image of hard carbon anode.

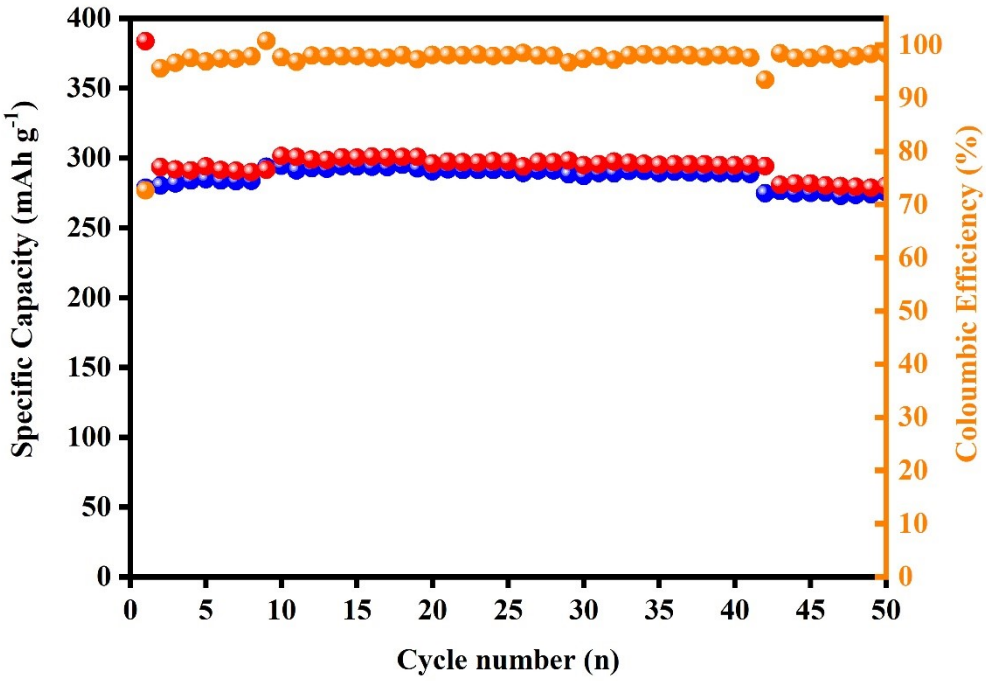

Fig. S16 The cycling performance of hard carbon anode in half-cell.

Table S1 Ionic radii and roles of metal elements.

	Li^{1+}	Fe^{3+}	Co^{3+}	Ni^{2+}	Ti^{4+}	Sn^{4+}
ionic radius (Å)	0.76	0.645	0.61	0.69	0.605	0.69
roles	stabilize structure	charge compensation	charge compensation	charge compensation	supporting structure	increase the operating potential

Table S2 ICP-MS result of transition metal elements in O3-NFCNTSL cathode material.

Theoretical chemical formula	Measured atomic ratio				
$Na(Fe_{0.2}Co_{0.2}Ni_{0.2}Ti_{0.2}Sn_{0.1}Li_{0.1})O_2$	Fe	Co	Ni	Ti	Sn
	0.20	0.21	0.22	0.20	0.10

Table S3 Crystallographic and Rietveld refinement data of O3-NFCNTSL cathode.

a(Å)	b(Å)	c(Å)	alpha	beta	gamma	volume(Å^3)	Space group
2.994276	2.994276	16.09147	90	90	120	124.942	R-3m
Label	Elem	Mult	x	y	z	Frac	Uiso
Na1	Na+1	3	0	0	0	0.985	0.0395
Fe2	Fe+3	3	0	0	0.5	0.2	0.1
O1	O-2	6	0	0	0.263642	0.91	0.01
Ni3	Ni+3	3	0	0	0.5	0.199	0.1
Co4	Co+3	3	0	0	0.5	0.2	0.1
Ti5	Ti+4	3	0	0	0.5	0.2	0.0286
Sn6	Sn+4	3	0	0	0.5	0.1	0.0068
Li7	Li+1	3	0	0	0.5	0.112	0.0679

Table S4 EDS report obtained from SEM of the as prepared material.

Element	Apparent concentration	K ratio	wt%	wt% Sigma	Atomic %	Standard sample label
O	17.80	0.05991	28.56	0.23	51.67	SiO_2
Na	8.41	0.03549	19.27	0.15	24.26	Albite
Ti	4.30	0.04300	8.80	0.11	5.31	Ti
Fe	5.11	0.05105	10.27	0.16	5.32	Fe
Co	5.45	0.05452	11.38	0.20	5.59	Co
Ni	5.04	0.05036	10.23	0.22	5.04	Ni
Sn	5.05	0.05054	11.50	0.17	2.80	Sn
Total			100.00		100.00	

Table S5 Co, Ni, Fe, and Ti K-edge EXAFS structural parameters of the pristine O3-NFCNTSL. (coordination numbers of Co-O, Ni-O, Fe-O, and Ti-O are 6)

Path	*r* / Å	σ^2 / 10^{-3} Å^2	$\triangle E$ / eV	*R*
Co-O	1.94(3)±0.044	3.56±0.71	-0.08±0.05	0.002
Co-M	2.91(1)±0.006	6.35±0.57		
Ni-O	2.06(3)±0.002	10.19±2.17	1.87±0.55	0.001
Ni-M	2.99(7)±0.057	10.54±1.42		
Fe-O	1.99(3)±0.067	9.12±3.17	2.80±1.02	0.002
Fe-M	2.95(2)±0.041	6.47±2.37		
Ti-O	1.97(6)±0.084	8.42±1.13	2.60±1.57	0.001
Ti-M	2.97(7)±0.035	4.54±1.24		

r: bond length; σ^2: Deby-Waller factor (disorder); $\triangle E$: inner shell potential shift; *R*: *R*-factor

Table S6 Co, Ni, Fe, and Ti K-edge EXAFS structural parameters of the O3-NFCNTSL at full charge of 4.1 V using P3 as model.

(coordination numbers of Co-O1, Ni-O1, Fe-O1, Co-O2, Ni-O2, and Fe-O2 are 3)

Path	*r* / Å	σ^2 / 10^{-3} Å^2	$\triangle E$ / eV	*R*
Co-O1	1.81(6)±0.126	-5.41±2.08		
Co-O2	1.95(6)±0.036	-5.88±0.89	-2.51±0.75	0.002
Co-M	2.91(1)±0.059	6.35±0.57		
Ni-O1	1.85(6)±0.038	2.37±0.73		
Ni-O2	2.00(3) ±0.010	2.08±1.46	-1.64±0.40	0.004
Ni-M	2.85(4)±0.043	10.65±4.37		
Fe-O1	1.91(7)±0.026	2.27±1.22	-2.60±1.53	0.001
Fe-O2	2.05(8)±0.051	3.85±2.56		
Fe-M	2.87(2)±0.026	14.22±2.09		

r: bond length; σ^2: Deby-Waller factor (disorder); $\triangle E$: inner shell potential shift; *R*: *R*-factor

Table S7 Co, Ni, Fe, and Ti K-edge EXAFS structural parameters of the O3-NFCNTSL at full charge of 2.0 V using O3 as model.

(coordination numbers of Co-O, Ni-O, and Fe-1are 6)

Path	r / Å	σ^2 / 10^{-3} Å^2	$\triangle E$ / eV	R
Co-O	1.93(5)±0.012	4.20±0.94	-0.68±0.29	0.003
Co-M	2.89(7)±0.096	6.37±0.74		
Ni-O	2.04(2)±0.018	14.88±2.20	-1.26±0.01	0.001
Ni-M	2.92(6)±0.067	10.98±1.18		
Fe-O	1.98(6)±0.074	9.08±3.16	-3.12±3.47	0.002
Fe-M	2.94(0)±0.054	6.30±2.44	-2.71±0.09	

r: bond length; σ^2: Deby-Waller factor (disorder); $\triangle E$: inner shell potential shift; R: R-factor

Table S8 Electrochemical performance of cathode materials for sodium ion batteries in recent years.

Electrode materials	Initial capacity @ 0.1C (mAh g^{-1})	Cycle retention (rate/number/retention)	Rate performance (mAh g^{-1})	Ref.
$NaNi_{0.2}Mn_{0.2}Fe_{0.6}O_2$	112.5	0.1C/100/81%	/	6
$NaFeO_2$	85	0.1C/100/80%	2C/75	7
$NaFe_{0.55}Mn_{0.45}O_2$	102.2	0.1C/200/10.3%	/	8
$Na_{9/10}Cr_{1/2}Fe_{1/2}O_2$	129	0.1C/100/69%	2C/86	9
$Na_{0.67}Cu_{0.28}Mn_{0.72}O_2$	109	1C/ 50 /98%	5C/76	10
$Na[Ni_{0.60}Mn_{0.35}Co_{0.05}]O_2$	151	0.2C/120/55%	1C/91	11
$Na_{2/3}Ni_{1/3}Mn_{2/3}O_2$	67	0.1C/50/88.7%	1C/100	12
$Na_{0.59}Co_{0.10}Mn_{0.90}O_2$	164.27	5C/1000/74.2%	/	13
$Na_{0.67}Ni_{0.17}Ti_{0.08}Mn_{0.67}O_2$	125	0.1C/50/83.5%	1C/80	14
$Na_{0.9}Mn_{0.55}Ni_{0.35}Cu_{0.1}O_2$	168	0.1C/100/71%	2C/121	15
$NaFe_{0.45}Co_{0.45}Ti_{0.1}O_2$	144	0.1C/50/70%	/	16
$Na_{0.67}Ni_{0.18}Mg_{0.15}Mn_{0.67}O_2$	123	0.1C/100/92%	20C/67	17
$Na(Fe_{0.2}Co_{0.2}Ni_{0.2}Ti_{0.2}Sn_{0.1}Li_{0.1})$	108.6	0.5C/100/80%	2C/80.8	This work

Table S9 The results of linear fitting concerning peak current versus square root of the scan rate at different oxidation and reduction peaks of O3-NFCNTSL electrode.

Equation	y = a + b*x	
Plot	cathodic scan	anodic scan
Weight	No Weighting	
Intercept	-2.11957E-4 ± 2.19875E-5	1.58766E-4 ± 2.15517E-5
Slope	0.03762 ± 9.83312E-4	-0.03088 ± 9.6382E-4
Residual Sum of Squares	1.30245E-9	1.25132E-9
Pearson's r	0.99864	-0.99806

Table S10 The results of linear fitting concerning voltage versus square root of the galvanostatic time.

Equation	y = a + b*x
Plot	Fig.4 c
Weight	No Weighting
Intercept	3.30101 ± 9.04318E-4
Slope	0.00308 ± 3.01439E-5
Residual Sum of Squares	0.00301
Pearson's r	0.99156
R-Square (COD)	0.98319
Adj. R-Square	0.98309

Table S11 Na^+ diffusion coefficients of cathode materials for sodium ion batteries in recent years.

Cathode materials	**D (cm^2 s^{-1})**	**Method**	**Ref.**
P2-$Na_{0.8}Li_{0.1}Mn_{0.6}Ni_{0.2}Cu_{0.1}O_2$	1.0 - 2.0×10^{-10}	GITT	18
O3-$NaNi_{1/4}Co_{1/4}Fe_{1/4}Ti_{1/4}O_2$	1.64 × 10^{-11}	CV	19
O3-$NaNi_{0.12}Cu_{0.12}Mg_{0.12}Fe_{0.15}Co_{0.15}Mn_{0.1}Ti_{0.1}Sn_{0.1}Sb_{0.04}O_2$	4 × 10^{-11}	GITT	20
P2-$Na_{0.67}Mn_{0.55}Ni_{0.25}Ti_{0.1}Li_{0.1}O_2$	8.82 × 10^{-14}	PITT	21
Tunnel-$[Na_{0.396}Li_{0.044}][Mn_{0.97}Li_{0.03}]O_2$	1.6 × 10^{-10}	GITT	22
P2-$Na_{2/3}Cu_{1/12}Ni_{1/4}Mn_{2/3}O_2$	10^{-12} - 10^{-10}	GITT	23
P2-$Na_{2/3}Mn_{1/2}Co_{1/3}Cu_{1/6}O_2$	1.465 × 10^{-12}	GITT	24
P2-$Na_{0.67}Mn_{0.5}Co_{0.4}Fe_{0.1}O_2$	0.8 × 10^{-13} - 0.9 × 10^{-11}	GITT	25
O3-$NaMn_{0.5}Ni_{0.5}O_2$	2.49 × 10^{-12}	GITT	26
O3-$Na_{0.93}Li_{0.12}Ni_{0.25}Fe_{0.15}Mn_{0.48}O_2$	1 × 10^{-11} - 5 × 10^{-11}	GITT	27
O3-$Na_{0.75}Fe_{0.2}Cu_{0.3}Mn_{0.5}O_2$	1.51 × 10^{-11}	GITT	28
O3-$Na_{0.8}Ni_{0.6}Sb_{0.4}O_2$	10^{-12} - 10^{-11}	GITT	29
O3-$NaNi_{0.35}Fe_{0.2}Mg_{0.05}Mn_{0.4}O_2$	4.0886 × 10^{-11}	CV	30
O3-$NaNi_{0.45}Mn_{0.3}Ti_{0.2}Zr_{0.05}O_2$	1.28 × 10^{-14}	EIS	31
P2-$Na_{2/3}Li_{1/9}[Ni_{2/9}Li_{1/9}Mn_{2/3}]O_2$	2.19 × 10^{-13}	EIS	32
P2-$Na_{0.59}Co_{0.1}0Mn_{0.85}(Ti_2V)_{0.05}O_2$	1.559 ×10^{-12}	CV	33
O3-$Na(Fe_{0.2}Co_{0.2}Ni_{0.2}Ti_{0.2}Sn_{0.1}Li_{0.1})O_2$	5.75×10^{-11}	GITT	This work

Table S12 Lattice parameters evolution of O3-NFCNTSL at different voltages.

Voltage status	a (Å)	b (Å)	c (Å)	V (Å^3)
initail (2.0V)	2.998	2.998	16.1334	125.2
discharge to 2.0V	2.9901	2.9901	16.1334	124.92

Reference:

[1] J. L. Yue, Y. N. Zhou, X. Yu, S. M. Bak, X. Q. Yang and Z. W. Fu, J. Mater. Chem. A, 2015, 3, 23261-23267.

[2] J. L. Yue, W. W. Yin, M. H. Cao, S. Zulipiya, Y. N. Zhou and Z. W. Fu, Chem. C, 2015, 51, 15712.

[3] M. Sathiya, Q. Jacquet, M. L. Doublet, O. M. Karakulina, J. Hadermann and J. M. Tarascon, Adv. Energy Mater., 2018, 8, 1702599.

[4] J. B. Goodenough, Mol. Cryst. Liq. Cryst., 2006, 311, 1-14.

[5] Y. You, S. Xin, H. Y. Asl, W. Li, P. F. Wang, Y. G. Guo and A. Manthiram, Chem., 2018, 4, 2124-2139.

[6] J. Feng, S. H. Luo, Y. Dou, J. Cong, X. Liu, P. Li, S. Yan, Q. Wang, Y. Zhang, X. Lei and J. Gao, J. Electroanal. Chem., 2022, 914, 116301.

[7] J. Xu, Z. Han, K. Jiang, P. Bai, Y. Liang, X. Zhang, P. Wang, S. Guo and H. Zhou, Small, 2020, 16, e1904388.

[8] L. Zhang, T. Yuan, L. Soule, H. Sun, Y. Pang, J. Yang and S. Zheng, ACS Appl. Energy Mater., 2020, 3, 3770-3778.

[9] R. Li, Y. Liu, Z. Wang and J. Li, Electrochim. Acta, 2019, 318, 14-22.

[10] W. Zheng, Q. Liu, Z. Wang, Z. Wu, S. Gu, L. Cao, K. Zhang, J. Fransaer and Z. Lu, Energy Stor. Mater., 2020, 28, 300-306.

[11] R. Mishra, S. K. Singh, H. Gupta, N. Srivastava, D. Meghnani, R. K. Tiwari, A. Patel, A. Tiwari, V. K. Tiwari and R. K. Singh, Appl. Surf. Sci., 2021, 535, 147695.

[12] H. Liu, X. Gao, J. Chen, J. Gao, S. Yin, S. Zhang, L. Yang, S. Fang, Y. Mei, X. Xiao, L. Chen, W. Deng, F. Li, G. Zou, H. Hou and X. Ji, J. Power Sources, 2021, 508, 230324.

[13] J. Deng, Y. Wang, Z. Wang, J. Li and Y. Luo, Chem. Phys. Lett., 2021, 783, 139050.

[14] D. Pahari and S. Puravankara, J. Power Sources, 2020, 455, 227957.

[15] M. Kouthaman, P. Arjunan, K. Kannan, V. Priyanka, R. Subadevi, V. Kumaran, R. M. Gnanamuthu and M. Sivakumar, J Taiwan Inst Chem Eng, 2020, 117, 86-92.

[16] M. Kouthaman, K. Kannan, P. Arjunan, T. Meenatchi, R. Subadevi and M. Sivakumar, Mater. Lett., 2020, 276, 128181.

[17] J. Feng, S. H. Luo, J. Wang, P. Li, S. Yan, J. Li, P. Q. Hou, Q. Wang, Y. Zhang and X. Liu, ACS Sustain. Chem. Eng., 2022, 10, 4994-5004.

[18] T. Chen, J. Guo, Y. Zhuo, H. Hu, W. Liu, F. Liu, P. Liu, J. Yan and K. Liu, Energy Stor. Mater., 2019, 20, 263-268.

[19] J. L. Yue, Y. N. Zhou, X. Yu, S. M. Bak, X. Q. Yang and Z. W. Fu, J. Mater. Chem. A, 2015, 3, 23261-23267.

[20] C. Zhao, F. Ding, Y. Lu, L. Chen and Y. Hu, Angew. Chem. Int. Ed, 2020, 59, 264-269.

[21] Z. Y. Li, J. Zhang, R. Gao, H. Zhang, L. Zheng, Z. Hu and X. Liu, J. Phys. Chem. C, 2016, 120, 9007-9016.

[22] X. Liang, H. Kim, H. G. Jung and Y. K. Sun, Adv. Funct. Mater., 2021, 31, 2008569.

[23] L. Zheng, J. Li and M. Obrovac, Chem. Mater., 2017, 29, 1623-1631.

[24] W. L. Pang, J. Z. Guo, X. H. Zhang, C. Y. Fan, X. J. Nie, H. Y. Yu, W. H. Li, Q. Yang and X. L. Wu, J. Alloys Compd., 2019, 790, 1092-1100.

[25] S. Chu, C. Zhang, H. Xu, S. Guo, P. Wang and H. Zhou, Angew. Chem., 2021, 60, 13366-13371.

[26] P. F. Wang, Y. You, Y. X. Yin and Y. G. Guo, J. Mater. Chem. A, 2016, 4, 17660-17664.

[27] X. G. Yuan, Y. J. Guo, L. Gan, X. A. Yang, W. H. He, X. S. Zhang, Y. X. Yin, S. Xin, H. R. Yao, Z. Huang and Y. G. Guo, Adv. Funct. Mater., 2022, 32, 2111466.

[28] T. T. Wei, N. Zhang, Y. S. Zhao, Y. R. Zhu and T. F. Yi, Compos. B. Eng., 2022, 238, 109912.

[29] L. Yu, X. X. Xing, S. Y. Zhang, X. Zhang, X. Han, P. F. Wang and S. Xu, ACS Appl. Mater. Interfaces, 2021, 13, 32948-32956.

[30] X. Zhang, Y. N. Zhou, L. Yu, S. Y. Zhang, X. X. Xing, W. Wang and S. Xu, Mater. Chem. Front., 2021, 5, 5344-5350.

[31] M. Leng, J. Bi, W. Wang, Z. Xing, W. Yan, X. Gao, J. Wang and R. Liu, J. Alloys Compd., 2021, 855,157533.

[32] Z. Y. Li, X. Ma, K. Sun, L. He, Y. Li and D. Chen, ACS Appl. Energy Mater., 2021, 5, 1126-1135.

[33] J. Deng, Y. Wang, Z. Wang, J. Li and Y. Luo, Chem. Phys. Lett., 2021, 783 ,139050.